Journal of Radioanalytical and Nuclear Chemistry
https://doi.org/10.1007/s10967-024-09548-w

Agmatine ligand functionalized magnetic alginate beads for removal of U(VI) ions from solution

Gulay Bayramoglu[1,2] · **Mehmet Yakup Arica**[1]

Received: 10 March 2024 / Accepted: 6 May 2024
© The Author(s) 2024

Abstract
In the presented work, magnetic alginate (MA) beads were prepared and activated with epichlorohydrin and then functionalized with agmatine ligands (MA-A). The materials were analyzed by FTIR, SEM, XRD, and BET methods. The adsorption capacity of the MA-A for U(VI) was 451.4 mg/g. The Langmuir isotherm model well described the experimental data for the adsorption of U(VI) ions. The second-order kinetic model data proposed that the adsorption of U(VI) ions preferred the chemisorption mechanism. The adsorption enthalpy of the MA-A beads for U(VI) ions was 35.4 kJ/mol. After seven cycles of use, the adsorption capacity of MA-A beads was not significantly changed for U(VI) ions. Finally, the functionalization of MA beads with agmatine ligand can be a good candidate for applications for environmental technologies to remove metal ions.

Keywords Magnetic nanoparticles · Magnetic alginate beads · Agmatine ligand · U(VI) · Adsorption

Introduction

Uranium (VI) ions cause strict risks at even low concentrations for living organisms and human health [1–4]. U(VI) ions have initiated widespread alarm due to their high toxicity and robust carcinogenicity [5–7]. Therefore, removing U(VI) from the solution is necessary for human health. Thus, the hazardous effect of this metal ion is reduced [8, 9]. Many methods have been established to remove U(VI) ions from wastewater, such as solvent extraction, precipitation, and adsorption [10–14]. Among them, the adsorption method is easy and cheap [14]. The method could be easily used for wastewater treatment, and active carbon, clay minerals, ion exchange resins, functionalized biopolymers, and many adsorbents from biological origin were employed for the adsorption of metal ions from solutions [11, 15–17]. Alginate is a natural polysaccharide obtained from brown algae [18]. It has been used in many studies to prepare hydrogel adsorbents. It is a non-toxic, biodegradable, and cheap material [19, 20]. Recently, various functionalized alginate based adsorbents have been used for the adsorption of pollutants from solutions [6, 13]. Furthermore, using alginate-based materials as adsorbents has many advantages, such as being abundant in nature, cheap, and easy modification. These properties reveal a promising prospect for alginate based adsorbent for removal of pollutants [21]. The alginate has many –OH and carboxyl groups; the latter one on the polymer provides a sol–gel transition in the presence of multivalent cations such as calcium ions [22]. In addition, Fe_3O_4-incorporated adsorbents provide easy separation of the material from the solution after the adsorption of pollutants from wastewater [23–25]. Various alginate based adsorbents were prepared and used for the removal of organic and inorganic pollutants from wastewaters [6, 13, 26–28]. For example, glycine functionalized magnetic alginate beads were used for the adsorption of Hg(II) from an aqueous medium [6]. Magnetic nanoparticles entrapped alginate/polyvinyl alcohol composite beads were prepared, and the adsorption efficiency of Pb(II) was evaluated [21]. Methionine functionalized magnetic alginate was synthesized and used for the effective elimination of arsenic from water [20]. In another study, magnetic alginate activated carbon beads were prepared and Cd(II), Hg(II) and Ni(II) ions removal performance were tested on mono-metal and ternary systems [22]. Magnetic alginate nanoparticles were synthesized and tested for Methylene Blue adsorption–desorption [24].

✉ Gulay Bayramoglu
g_bayramoglu@hotmail.com

[1] Biochemical Processing and Biomaterial Research Laboratory, Gazi University, 06500 Teknikokullar, Ankara, Turkey

[2] Department of Chemistry, Faculty of Sciences, Gazi University, 06500 Teknikokullar, Ankara, Turkey

Published online: 21 May 2024

Calcium alginate coated chitosan hydrochloride hydrogel beads were prepared and used for the removal of Cu(II) and U(VI) from aqueous solutions [13].

In the presented work, the magnetic alginate beads were prepared by ionic cross-linking with Ca(II) ions, activated with eprichlorohydrin, and then functionalized with agmatine, which has an aminoguanidine group. To our best knowledge, no study has been reported with agmatine functionalized magnetic alginate beads for removing U(VI) ions. The prepared adsorbent has four amines (primary and secondary amine groups) and many carboxyl and hydroxyl groups. These amine groups are protonated to positively charged groups in acidic and neutral mediums, resulting in positively charged surfaces to remove metal ions. Herein, the amine, carboxyl, and hydroxyl groups can interact with U(VI) ions via chelating and ion exchange mechanisms. The efficiency of U(VI) adsorption by the MA-A beads were investigated. Moreover, the impact of six parameters, namely adsorption amount, adsorption time, ionic strength, medium pH, initial metal ions concentration, and temperature, on the adsorption performance was studied. Later, the experimental adsorption data were used to evaluate adsorption isotherms, kinetics, and thermodynamic parameters. This present study can offer important guidelines for preparing a cheap adsorbent to eliminate toxic metal ions from wastewater.

Materials and methods

Materials

Alginic acid sodium salt from brown algae, agmatine sulfate salt, arsenazo(III), and epichlorohydrin were obtained from Sigma–Aldrich (Hamburg, Germany). U(VI) was obtained from Riedel-de-Haen AG (Germany). Ammonia solution, H_2SO_4 (98%), H_2O_2 (30%), $KMnO_4$, $FeCl_3 6{\cdot}H_2O$, $FeCl_2 4{\cdot}H_2O$ were supplied from Sigma–Aldrich. All these chemicals were used as received in the experimental work.

Preparation of magnetic nanoparticles

The magnetic nanoparticles (MNP) were synthesized as described previously [25]. Briefly, $FeCl_3$ solution (200 mL, 0.3 mol/L) and $FeSO_4$ (250 mL, 0.1 mol/L) were added to a reaction vessel agitated at room temperature for 1.0 h. Then, the reaction temperature was raised to 70 °C, then 200 mL of NH_4OH (0.1 mol/L) was added to the reaction mixture and refluxed for 2.0 h. After this period, the temperature was elevated to 90 °C further refluxed about 1.0 h. Then, the magnetic nanoparticles were collected using an external magnet, washed with purified water, and dried under reduced pressure.

Preparation of magnetic alginate beads

Na-alginate (2.0 g) was dissolved in distilled water, then, 2.0 g of MNP were added and stirred for about 1.0 h. The mixture was dropped into $CaCl_2$ solution (0.1 mol/L) with a burette, and the curing solution was stirred to prevent the aggregation of the magnetic nanoparticles that entrap in the Ca-alginate beads. The magnetic alginate beads (~1.0 mm in diameter) were stirred for a further 1.0 h. The beads were collected with an external magnet and washed twice with 200 mL of deionized water. Then, the magnetic beads were collected with an external magnet and incubated in deionized water for 24 h, and the process was repeated twice. Then, the magnetic alginate beads (5.0 g), NaCl (50 mL, 10%, w/w), and NaOH solution (50 mL, 10%, w/w) were added into a reactor and stirred at room temperature for 15 min. After this period, for functionalization of the magnetic beads surface with epoxy groups, epichlorohydrin (5.0 mL) was added to this mixture drop by drop within 10 min. The reactor temperature was raised to 65 °C and stirred for 3.0 h. The epoxy groups functionalized magnetic alginate beads were collected and washed with deionized water and 70% ethanol.

For immobilization of agmatine ligand on the activated MA beads, agmatine sulfate (1.0 g) was dissolved in deionized water (50 mL) and combined with MA beads (5.0 g) in ethanol solution (70%, 50 mL). The reaction was carried out in a reactor at 65 °C, stirred magnetically for 3.0 h. A chemical reaction took place between the amino group of the agmatine and the epoxy groups of the activated magnetic alginate beads. To remove the non-specifically interacted agmatine molecules, the functionalized beads were washed with deionized water and sonicated for 5 min in ethanol solution (70%) using an ultrasonic bath. The amount of attached agmatine was determined with potentiometric titration.

Bare MA beads were prepared by hydrolyzing epoxy groups of the activated MA beads in H_2SO_4 solution (0.5 mol/L, 50 mL) at 50 °C for 2.0 h. It was used as a control for adsorption of uranyl ions. The MA-A beads were stored at 4 °C until use. A schematic representation of the preparation of MA-A beads is presented in Fig. 1.

Characterization of magnetic alginate beads

The bare MA and modified MA-A bead surface properties were obtained using SEM. The FTIR spectra of the materials were obtained using Nicolet TM ISTM 50 FTIR spectrometer (Thermo Fisher Scientific, USA). The magnetic properties of the MNP nanoparticles and MA-A were examined using a VSM (VSM, 880; ADE Technologies,

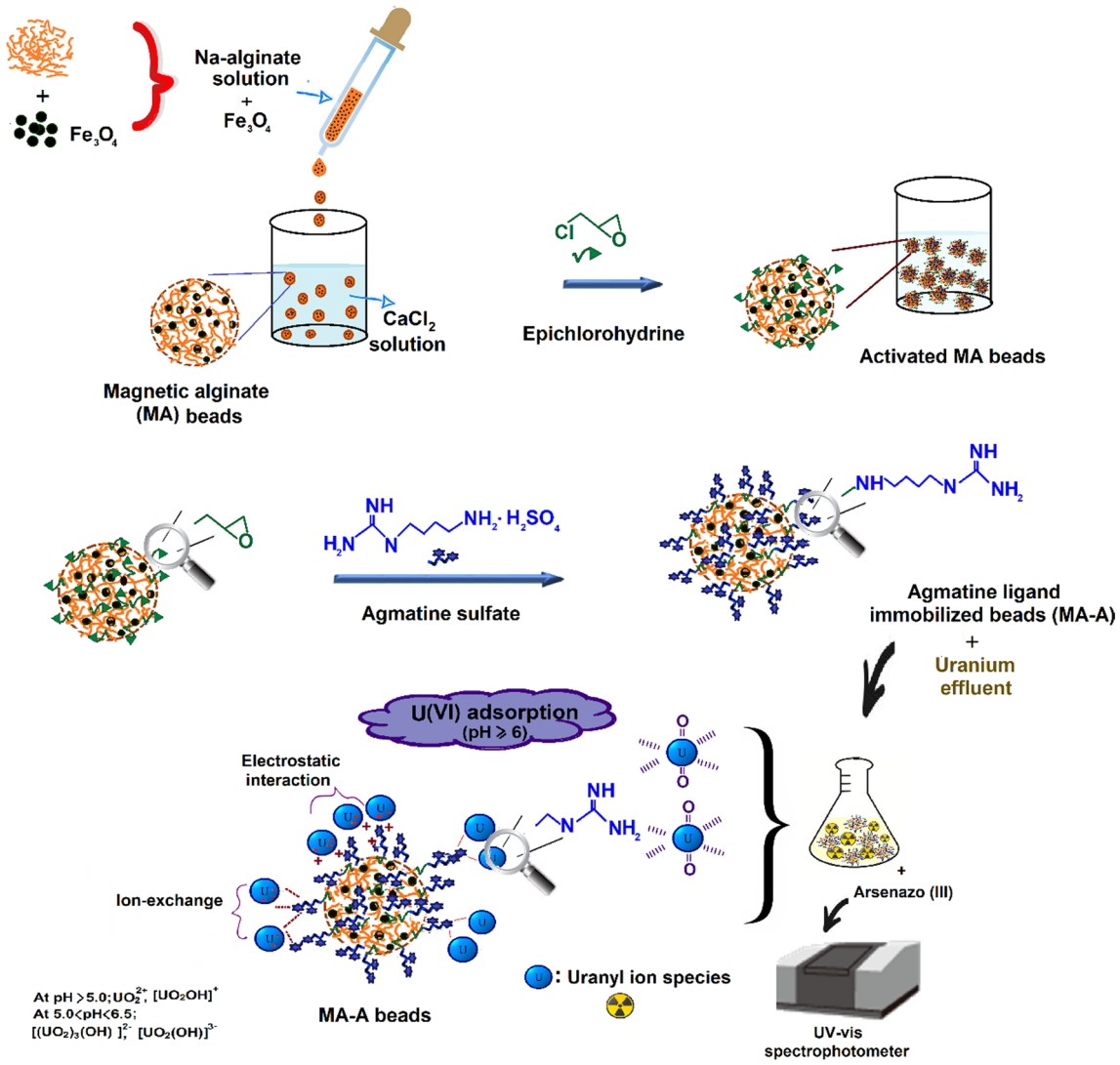


Fig. 1 Schematic representation of the preparation of the adsorbent

USA). The zeta potential measurements of the MA and modified MA-A beads at different pH values were obtained with a Zetasizer (Nano ZS, Malvern Instruments Ltd). The surface area and average pore size of the samples were studied by the Brunauer–Emmett–Teller (BET) analysis. The N_2 adsorption–desorption experiments were realized using ASAP2020 HD88. The amount of attached agmatine was determined with potentiometric titration. For this, the sample beads (0.2 g) were transferred to a flask containing HCl solution (10 mL, 50 mmol/L). The flask was placed on a shaker and rotated at 40 °C for about 4 h. The sample beads were magnetically collected and washed with deionized water. The filtrate and washed solution were added into a volumetric flask (250 mL) and completed with distilled water. The remaining HCl content of the solution was determined by potentiometric titration with NaOH solution (100 mmol/L).

Adsorption studies

The adsorption experiments of U(VI) ions on the MA-A beads were studied using the bare alginate beads as a control. The solutions containing U(VI) ions (100 mL) were added to a flask containing 50 mg MA-A beads, and then it was located in a shaker and operated at 150 rpm and 25 °C for 3 h. The medium pH was varied between 3.0 and 9.0, and the initial concentration of U(VI) ions was between 10 and 400 mg/L. The influence of the adsorbent amount on the adsorption performance was performed by changing the adsorbent dose between 0.1 and 1.5 g/L. The adsorption isotherms were obtained with 50 mg of adsorbent into a solution of U(VI) ions with different initial concentrations. After adsorption equilibrium, the adsorbents were regenerated by 50 mmol/L HNO_3 solution. The concentrations of remaining U(VI) ions in the adsorption medium

were determined at 651 nm, after complexation with the arsenazo (III) [29–32].

Results and discussions

Properties of prepared magnetic alginate beads

The preparation of the MA and modified MA-A beads is presented in Fig. 1. The epoxy groups of the activated MA beads were reacted with the amine group of the agmatine ligand via a ring-opening reaction. The number of available epoxy groups on the activated MA beads was 4.1 mmol/g by the pyridine–HCl method [25]. The number of amine groups on the MA-A beads was found to be 11.9 mmol/g. The surface area and pore size of the MA-A beads are very important when removing metal ions. The surface area and pore size of the bare MA and MA-A beads were determined as 28.9 m^2 /g and 1.7 nm, and 24.5 m^2 /g and 1.3 nm, respectively. After grafting the MA beads with agmatine ligand, the specific surface area and pore size were significantly reduced.

The information about the chemical structure of the MA and modified MA-A beads was obtained using an FTIR spectrometer in the range of 400–4000 cm^{-1} (Fig. 2). The FTIR spectra of the MA are presented in Fig. 2A. The hydroxyl group and CH_2 stretching vibration peaks were observed at 3282 and 2358 cm^{-1}, respectively. The carboxyl group peak was detected at 1587 cm^{-1}. The mannuronic acid and uronic acid functional groups were observed at 935 cm^{-1} and the at wavenumber 1024 cm^{-1}, respectively. The observed peaks at 631 and 600 cm^{-1} were attributed to the Fe_3O_4 nanoparticles in alginate beads. As seen in Fig. 2B, the FT-IR analysis of the samples provided strong evidence of the successful preparation of the MA-A beads. For example, the peak at 1441 cm^{-1} was due to the characteristic peak of C–N in the agmatine structure. The characteristic adsorption peak of –NH was detected at 1378 cm^1, which proved that agmatine was covalently attached to alginate. These observed new peaks were evidence of the attachment of agmatine molecules to the MA beads via epoxy groups of epichlorohydrin.

The SEM images were acquired to estimate the morphologic properties of the MA-A beads (Figs. 3). MNP entrapped alginate had a nearly spherical morphology of around 1.0 cm in diameter. The MA-A beads showed an irregular microstructure.

VSM data was obtained to show the magnetic properties of the MNP and MA-A beads. The magnetic hysteresis loop curves of the MNP and MA-A beads were obtained S-shaped over the involved magnetic field, representing that the used materials had magnetic properties (Fig. 4). The magnetic presentation of the MNP and MA-A beads were 44.8 and 22.7 emu/g, respectively. The magnetic property of the MA-A decreased due to the presence of non-magnetic material.

Effect of adsorbent dosage on adsorption performance of MA-A beads for U(VI) ions

One of the major limitations of using MA-A beads for large-scale application removal of U(VI) ions is the adsorbent dosage in the medium. The effect of the adsorbent amount on the adsorption performance was realized by varying the adsorbent amount in the range of 0.25–1.5 g/L at 200 mg/L metal ion concentration. From Fig. 5, the amounts of U(VI)

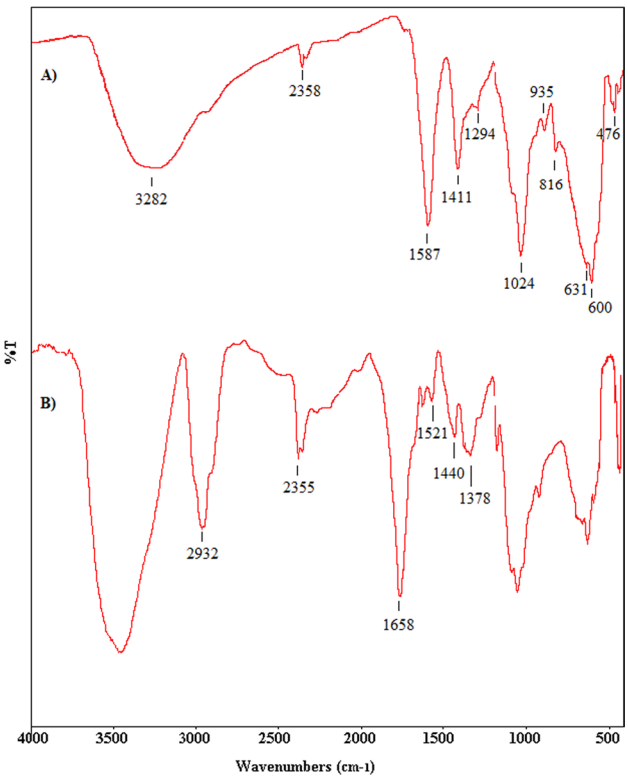


Fig. 2 FTIR spectra: MA beads (**A**), and MA-A beads (**B**)

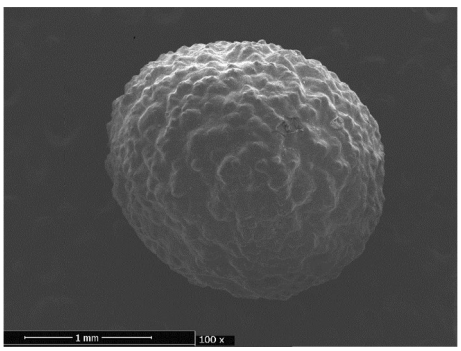


Fig. 3 SEM micrograph of the MA-A beads at100× magnification

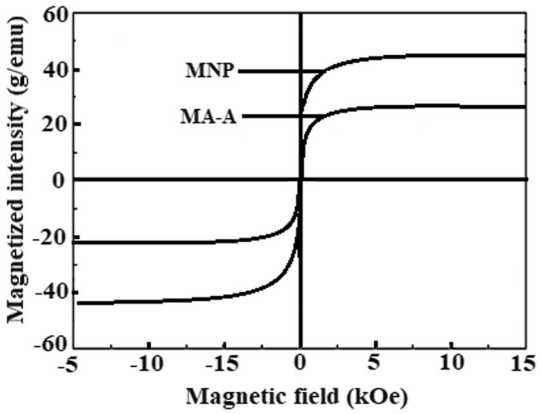


Fig. 4 VSM patterns of MNP and MA-A beads

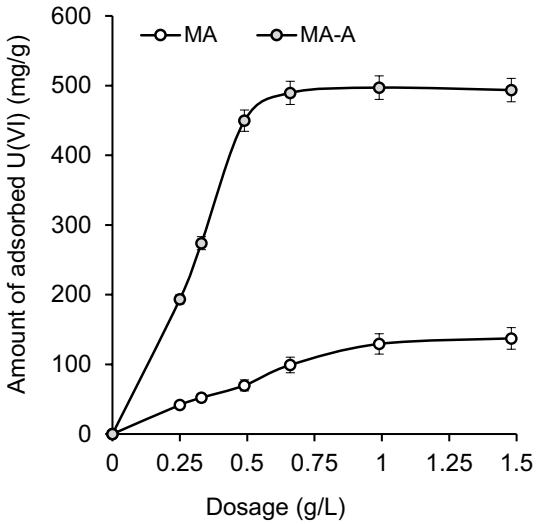


Fig. 5 Effect of adsorbents dosage on U(VI) ions removal performance of the MA and MA-A beads

ions removal increased from 41.7 to 137.2 mg/g as MA beads raised from 0.25 to 1.5 g/L. Thus, a rise in the adsorption amount was observed with increases in the sorbent dosage. This increase in the adsorption efficiency of U(VI) ions could result from increased adsorbent in the medium. At the same time, the adsorbed amounts of U(VI) ions per unit of sorbents were decreased with increasing amounts of the adsorbent. The reduction in the adsorption efficiency of the used adsorbent can be due to the adsorptive sites of the sorbent not completely occupied by the U(VI) ions [17].

Influence of NaCl concentration on the adsorption efficiency of the MA-A beads

The influence of increasing NaCl concentration on the adsorption efficiency of U(VI) ions on the MA and MA-A was realized by varying concentrations of NaCl in the

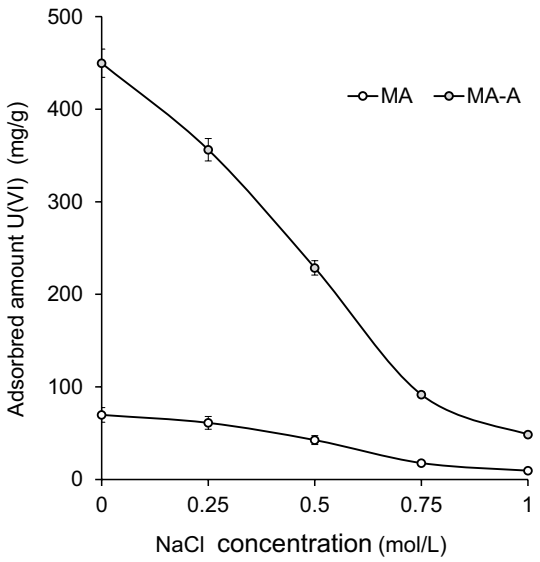


Fig. 6 Effect of ionic strength on U(VI) adsorption on the MA and MA-A beads. (Temperature, 25 °C; contact time, 120 min; stirring rate 150 rpm)

medium (Fig. 6). It should be noted that U(VI) ionic species impact electrostatics and complexation interaction with the adsorbents due to the presence of different adsorptive groups (such as primary and secondary amine groups and hydroxyl groups). As can be seen from Fig. 6, with increasing NaCl concentration in the medium, electrostatic interactions between influential groups of the adsorbents and U(VI) ions were reduced. The adsorbed U(VI) ions on the MA and MA-A beads decreased from 69.8 to 9.6 mg/g and 449.7 to 41.6 mg/g when the concentration of NaCl was raised from 0.0 to 1.0 mol/L, respectively. Na^+ and Cl^- ions in the solution can shadow the charged areas of the adsorbent. Accordingly, the adsorptive groups of sorbents can be compressed, causing a reduction in electrostatic interactions between adsorbate and adsorbent. In earlier works, parallel results have been reported. For example, the adsorption of U(VI) ions on the 2,5-diamino benzene sulfonic acid functionalized fungal biomasses was reduced with an increasing NaCl concentration in the solution due to the reduced electrostatic interaction [31]. A similar observation was also reported in a previous study [33].

Effect of solution pH on adsorption efficiency

Generally, the medium pH changed both the adsorbate species and the surface charges of the adsorbents, which caused a substantial effect on the removal of metal ions. The influence of pH on the adsorption performance of U(VI) ions by the MA and MA-A beads is presented in Fig. 7. As observed from this figure, a strong pH dependency was detected for removing both metals, which showed that the medium pH

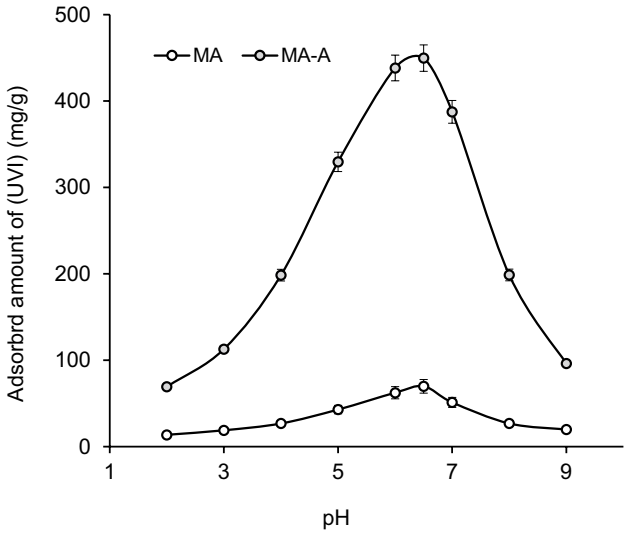


Fig. 7 Influence of pH on U(VI) adsorption performance of the MA and MA-A beads. (Temperature, 25 °C; contact time, 120 min; stirring rate 150 rpm)

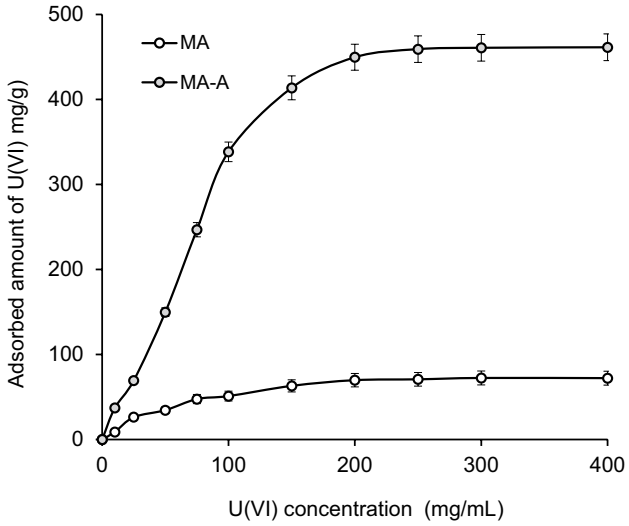


Fig. 8 Effect of initial concentration of on U(VI) adsorption on the MA and MA-A beads. (Temperature, 25 °C; stirring rate 150 rpm)

values played an essential role in removing U(VI) ions. The pKa_1, pKa_2 and pKa_3, values of the amine groups of agmatine are 2.25, 7.45, and 12.1, respectively, and could easily interact with the U(VI) ions in the studied pH range. In the pH range of 2.0–7.0, the amount of adsorbed U(VI) ions on the MA-A beads gradually increased with increasing pH value of medium and progressively decreased with increasing pH values. The highest adsorption capacity and removal efficiency for U(VI) ions on MA-A beads were observed at 6.5. At lower pH values, this could be explained by generating many protonated amine groups on the adsorbent surfaces, resulting in an electrostatic repulsion between positively charged uranyl ions and protonated amine groups. This resulted in a decrease in the amount of adsorbed U(VI) ions on the adsorbents. On the other hand, at $5.0 < pH < 7.0$, two anionic species are dominantly formed in this pH region: the polynuclear complex $(UO_2)_3(OH)^{2-}$ and the mononuclear complex $UO_2(OH)^{3-}$. These negatively charged uranyl ions species can interact with amine groups of the adsorbents. The maximum adsorption capacities were observed as 69.8 and 449.7 mg/g at pH 6.5 for the MA and MA-A beads, respectively. It should be noted that the significant forms of uranyl ions up to pH 5.0 are positively charged (i.e., UO_2^{2+}, UO_2OH^+, and $(UO_2)_2(OH)_2^{2+}$) [29, 33, 34]. Moreover, at low pH values, the high protonation of the adsorbent surfaces affected reinforced electrostatic repulsion for UO_2^{2+} ionic species. From these findings, the adsorption of uranium ions on MA-A beads could be considered mainly as coordination complex formation and ion exchange interaction. In an earlier study, parallel observations were reported; the maximum adsorption of U(VI) ions on oil-apatite nanoparticles was observed at pH 4.0 [35]. The amidoxime group-modified cross-linked benzyl polymer was applied for U(VI) adsorption, and the maximum adsorption was at pH 6.5 [36]. The polydopamine-functionalized polyamidoxime membranes were synthesized and tested for the removal of U(VI) ions. The maximum removal pH was attained at pH 5.0 [37]. Magnetite chitosan was modified with tetraethylenepentamine (TEPA) to remove U(VI) ions, and the maximum adsorption was achieved at pH 4.0 [38].

Adsorption isotherms studies

When the amount of metal ions in the solution was increased from 10 to 400 mg/L, the amount of U(VI) ions adsorbed on MA and MA-A beads increased. As is well known, the increasing amount of solute species in the solution medium is a driving force that increases the tendency to adhere to the energetic regions on the adsorbent. As a natural result of this effect, high adsorption capacity can be achieved for removing metal ions with a process whose adsorption tendency is promoted. In this context, a similar effect was observed on the uptake of U(VI) ions in the aqueous medium with the MA and MA-A beads, and the adsorption tendencies of these adsorbents increased proportionally depending on a certain concentration of the metal ion in the medium. It was determined that equilibrium was reached when the concentration value of 300 mg/L was reached. As reported above, this increase in adsorption capacity up to a certain concentration of the metal ion in the medium confirms that the binding sites for the target metal ions on the studied adsorbent are limited. The achieved equilibrium experimental adsorption capacities of the MA and MA-A beads were found to be for U(VI) ions 72.2 and 451.4 mg/g, respectively.

Finally, as observed in Fig. 8, the adsorption capacity of the U(VI) ions increased by 6.4 folds after agmatine ligand immobilization on the MA beads.

The adsorption performance of U(VI) ions by MA-A beads were tested by applying two theoretical adsorption isotherm models (i.e., Langmuir and Freundlich):

Langmuir model [39–41]:

$$q_e = q_m C_e / \left(K_d + C_e\right) \tag{1}$$

Freundlich isotherm model equation [42]

$$q_e = K_F \left(C_e\right)^{1/n} \tag{2}$$

The Langmuir plots were obtained for the adsorption of U(VI) ions on the MA-A beads at different temperatures, and the R^2 values were between 0.967 and 0.996. The calculated values (theoretical), q_m, for U(VI) on the MA-A beads agreed with the experimentally determined sorption capacity (q_{exp}) results (Table 1). Considering these results obtained using the Langmuir model, it has been shown that the adsorption of U(VI) ions on MA-A beads is probably dominated by the monolayer adsorption defined for homogeneous surfaces that reach equilibrium by saturating the energetic zones [43, 44].

The q_m value for U(VI) was calculated as 473.8 mg/g at 25 °C and at pH 6.5. Experimental data were also analyzed to remove U(VI) ions on the MA-A beads. The calculated model parameters (n and K_F) using Freundlich isotherm and the correlation coefficients (R^2) are presented in Table 1. The R^2 values determined at the studied temperatures showed that this isotherm model was unsuitable for both metal ions. Similarly, although it cannot be a direct result of the theoretical adsorption capacity of the adsorbent against the target analyst, the K_F value can be evaluated as the proportional adsorption amount under certain conditions.

Adsorption equilibrium time and kinetic-model analysis

In the adsorption process of U(VI) ions at an initial concentration of 200 mg/L onto MA-A beads, it was observed that the equilibrium time was reached rapidly in approximately 60 min. Figure 9 demonstrates the correlation between the contact time and adsorption amounts of onto MA-A beads. The adsorption trend of both metal ions onto MA-A beads as a function of time followed a gradual kinetics, where the adsorption trend was fast in the first 40 min, slow after that, and then equilibrium adsorption was reached within 60 min. During the adsorption period, as the binding sites of metal ions in the aqueous medium reached saturation, the removal rates of metals gradually decreased, and equilibrium adsorption was reached. It is reported in the literature that

Table 1 Langmuir and Freundlich isotherm models constants and correlation coefficients determined in the adsorption process of the adsorption of U(VI) ions to MA-A beads

T(K)	$q_{e,exp}$(mg/g)	Langmuir $[C_e/q_e = C_e/q_m + 1/K_a\, q_m]$				Freundlich $[lnq_e = lnK_F + 1/n\ lnC_e]$		
		q_m(mg/g)	$K_a \times 10^{-4}$(M^{-1})	R^2	*R_L	n	K_F(L/g)	R^2
288	369.7	382.8	0.37	0.967	0.174	1.55	9.35	0.974
298	451.4	473.8	0.48	0.995	0.132	1.71	16.8	0.962
308	511.2	532.5	0.61	0.993	0.089	1.86	24.1	0.958
318	614.7	655.7	0.98	0.996	0.068	1.93	37.3	0.949

* C_0 = 400 mg/L

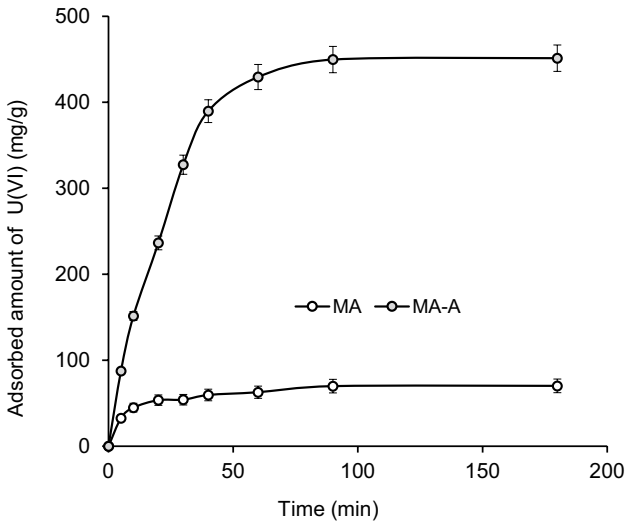


Fig. 9 Equilibrium adsorption time of U(VI) ions on MA and MA-A beads

equilibrium is reached in a more extended period for the removal of U(VI) and ions with different adsorbents used [44, 45]. It was found that with the MA-A beads in this study, a rapid adsorption equilibrium of U(VI) ions from an aqueous medium was achieved within a short processing time.

The first-order model Eq. [42]:

$$d_{qt}/d_t = k_1\left(q_e - q_t\right) \tag{3}$$

$$\log\left(q_e - q_t\right) = \log q_e - \left(k_1.t\right)/2.303 \tag{4}$$

The linear form of the second-order model Eq. [46]:

$$t/q_t = 1/\left(k_2 q_e^2\right) + t/q_e \tag{5}$$

By applying the experimental results obtained in U(VI) ions removal using MA-A beads to the first and second-order equation, R^2 values were found to be in the range of 0.993–0.998 (Table 2). These results showed that second-order kinetics describes the adsorption of U(VI) ions on MA-A beads. In addition, the theoretical adsorption capacity ($q_{e,\,cal}$) calculated from the second-order kinetic equation in the adsorption process of U(VI) ions on MA-A coincides well with the experimental results (q_e), confirming that this model is suitable. The chemical adsorption process could explain the adsorption process [43, 47], possibly because the polyamine and hydroxyl groups coordinate uranyl ions species on the adsorbent surfaces. It has been determined that the calculated (theoretical) adsorption capacity values calculated using MA-A beads for U(VI) ($q_{e,\,cal}$) vary depending on the temperature. By increasing the temperature of the adsorption medium from 288 to 318 K, the adsorption amounts of U(VI) increased from 369.7 to 614.5 mg/g for MA-A beads (Table 2).

Evaluation of thermodynamics of the adsorption system

As another critical parameter in the adsorption process, the effect of temperature on metal ion removal was investigated, and the adsorption capacity values determined for the removal of U(VI) ions using MA-A beads as a function of temperature are given in Table 3. As mentioned above, increasing the temperature of the adsorption system increases the adsorption capacity. Since the probability of collision of metal ions with the binding sites on the surface of MA-A beads increases with increasing temperature, the amount of U(VI) ions adsorbed to the adsorbent also increased. The fact that the adsorbed amounts of U(VI) ions depend on temperature indicates that the adsorption of

Table 3 Thermodynamic parameters for the adsorption of U(VI) MA-A beads

$[\Delta G^o = -RT\ ln\ K_a = \Delta H - T\Delta S^o][ln\ k_2 = lnA - E_a/RT]$				
T(K)	ΔG(kJ/mol)	ΔH(kJ/mol)	ΔS(kJ/mol K)	E_a(kJ/mol)
288	− 21.6			
298	− 23.5	35.4	0.179	− 12.3
308	− 25.2			
318	− 28.4			

Table 2 First and second-order kinetic constants for the adsorption of U(VI) ions to MA-A beads

T(K)	q_{exp}(mg/g)	First-order$[log(q_e\text{-}q_t) = logq_e - k_1 t/2.303]$			Second-order$[t/q_t = 1/(k_2\ q_e^2) + (t/q_e)]$			
		q_{eq}(mg/g)	$k_1 \times 10^2$(min^{-1})	R^2	q_{eq} (mg/g)	$k_2 \times 10^3$ (g/mg/min)	R^2	h(mg/g/min)
288	369.7	1331.7	12.4	0.948	383.9	0.19	0.998	23.5
298	451.4	1423.3	11.3	0.966	479.6	0.16	0.994	28.2
308	511.2	1695.2	12.2	0.954	532.3	0.14	0.996	33.7
318	614.5	1778.4	11.9	0.957	641.7	0.12	0.993	37.9

U(VI) ions on MA-A beads may be endothermic (Table 3). The Gibbs free energy change ($\Delta G°$) of adsorption U(VI) ions on the adsorbent was determined from the following equation:

$$\Delta G = -\mathrm{RT} \ln K_a \tag{6}$$

$$\ln K_a = -\Delta H/\mathrm{RT} + \Delta S/R \tag{7}$$

From Table 3, the negative ΔG values were achieved for the adsorption of both metal ions on the adsorbent, displaying that the adsorption courses of U(VI) ions on the adsorbent were spontaneous. Here, the ΔG values were in the range of between -21.6 and -28.4 for the adsorption of U(VI) ions on the MA-A beads. As illustrated in Table 3, as the temperature raised, the $\Delta G°$ values were obtained more talented, meaning that the higher temperature was more favorable for the adsorption of U(VI) ions. These results indicated that the adsorption of U(VI) ions on the adsorbent could be combined with physical/chemical or chemical adsorption. Similar findings have been reported in earlier studies with the presented thermodynamic variables [38, 39, 48, 49]. The positive ΔS values showed reduced randomness during the adsorption process of U(VI) ions, and both metal ions had a considerable affinity to the adsorbent. The positive value of $\Delta H°$ for the adsorption of U(VI) ions on the MA-A beads was found to be 35.4 kJ/mol^{-1}, proposing that the adsorption process of U(VI) ions on the adsorbent was endothermic and spontaneous.

Adsorption mechanisms of U(VI) ions on MA-A beads

Certain rules should first be made to understand the adsorption mechanism of U(VI) ions from the medium by the MA-A beads. The primary binding site of the MA-A beads is the agmatine group; this amine rich group has a high affinity to metal ions. The adsorbents adsorbed U(VI) ions with high affinity during adsorption, as observed from the above experimental results. As evidence EDS data were obtained from U(VI) ions laden MA-A beads by using bare MA-A beads as a control system (Fig. 10). The SEM images the obtaining EDXS, energy-dispersive-X-ray spectrum (EDXS) and SEM–EDX mapping analysis data for MA-A beads and MA-A-U(VI) beads are shown in Fig. 10A–C and D–F, respectively. As observed from Fig. 10, the energy-dispersive X-ray spectrums and elementals mappings were obtained to evaluate of elementals distribution of MA-A-U(VI) and bare MA-A beads. The uniformly distribution of agmatine coating and adsorbed uranyl ions on the beads surfaces were clearly seen from these data. Moreover, the uniform distribution of magnetic nanoparticles on the adsorbent surface provided an easy separation of uranyl ion laden adsorbent from the medium with an external magnet. From these observation, it can be said that the obtained data were clear evidence for adsorption of uranyl ions on the MA-A beads and the presence of adsorbed uranyl ions on the adsorbent. Also, the presence of functional groups for adsorption of U(VI) ions and sugested adsorption mechanism for the MA-A beads are presented in Fig. 11. As seen in this figure, the adsorption of U(VI) ions on the adsorbent could be take placed by the coordination complex and ion exchange mechanisms [47, 48]. As observed in Fig. 2, the MA-A beads had amine and hydroxyl group band at around 3400 cm^{-1} and two amine group peaks at 1441 and 1378 cm^{-1}. Besides, the carboxyl group peak of alginate was detected at 1658 cm^{-1}, and these functional groups could affect the performance of the as prepared adsorbent. Therefore, these functional groups may be responsible for the electrostatic interactions and affect the adsorption capacities of the MA-A beads for U(VI) ions. Thus, MA-A beads interact with U(VI) ions via coordination complexation and electrostatic interactions. These results suggested that the polyamine groups in the MA-A beads structure were dominant in the adsorption process of U(VI) ions.

U(VI) removal rate from the simulated seawater by MA-A beads

The performance of the MA-A beads was tested using simulated seawater spiked with various amounts of uranyl ions. The composition of the simulated seawater is presented in Table 4. Seawater has many metal ions, and the adsorbent's performance may be affected by these metal ion species. The effect of U(VI) ions concentration variation in the simulated seawater on the adsorption rate of MA-A beads was studied using the same seawater composition. Figure 12 shows that the adsorption performance of the adsorbent was positively affected by increasing the concentration of U(VI) ions from 25 to 200 g/L. The adsorption performance of the MA-A beads increased steadily with increasing spiked amounts of U(VI) ions, and the removal rate of U(VI) increased from 69 to 96%. As a result, the MA-A beads showed high U(VI) ions removal performance in artificial seawater at even low concentrations. These results showed that the prepared MA-A beads may be used to extract U(VI) ions from seawater.

Regeneration and repeated use

The repeated use of adsorbents in sequential cycles is an essential parameter, particularly for using adsorbents in industrial wastewater treatment. Therefore, U(VI) ions loaded on the MA-A beads were desorbed with a low concentration of HNO_3 (50 mmol/L) solution as previously described [17]. Adsorption–desorption cycles were realized seven times with the same adsorbent. During these

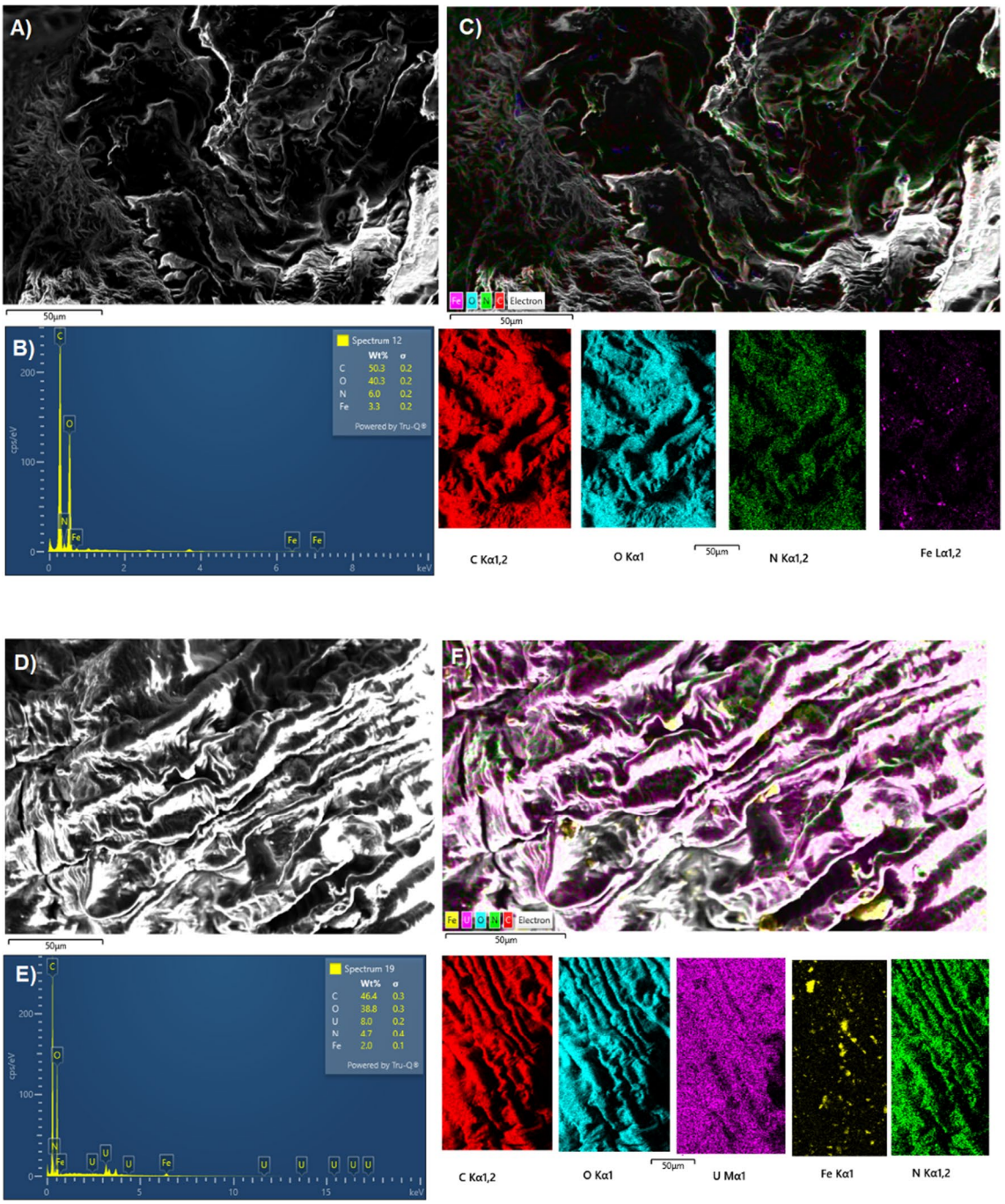


Fig. 10 SEM images, Energy-Dispersive-X-ray Spectrum and SEM–EDX mapping analysis of MA-A (partly, A, B, C) and MA-A-U(UVI) beads (partly, D, E, and F), respectively

successive cycles, MA-A beads sustained a nearly stable adsorption ratio about 96%, which protect its high physical and chemical stability in applications (Fig. 13), and the adsorption performance of MA-A beads for U(VI) was only decreased by about 4% (Fig. 13).

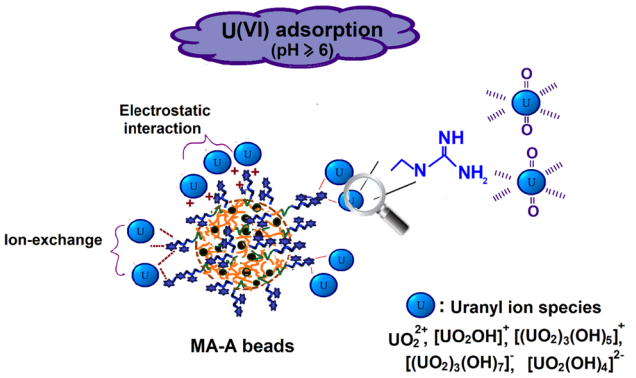


Fig. 11 The feasible adsorption mechanism of U(VI) on MA-A beads

Table 4 Concentrations of competing ions in simulated seawater

Metal ions	In seawater
Na(I)	10.8 g/L
Mg(II)	1.3 g/L
Ca(II)	440 mg/L
Fe(III)	1.7 µg/L
Cu(II)	1.0 µg/L
U(VI)	25–200 µg/L

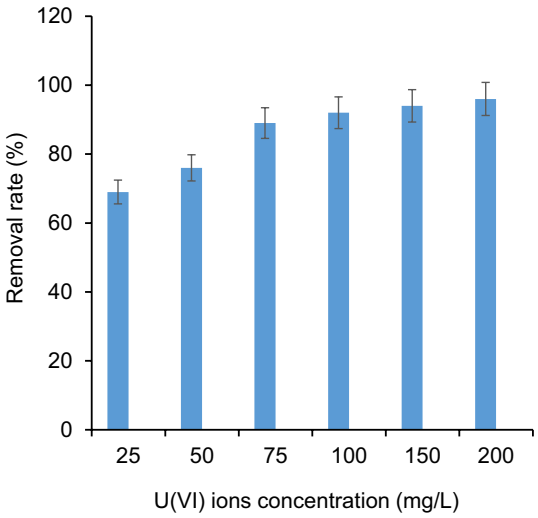


Fig. 12 Removal rate of U(VI) ions by MA-A beads from different amount U(VI) spiked simulated seawater

Comparison of MA-A beads with different adsorbents

The experimental adsorption capacity of the MA-A beads was compared to other adsorbent materials. As shown in Table 5, the adsorption capacity of the agmatine modified magnetic alginate beads had conspicuously higher adsorption capacity with respect to the most of adsorbents reported in the literature [2, 50–57]. This could be due to from electrostatic and coordination complex interactions between the several amine groups of agmatine ligand with available carboxyl groups of alginate polymer and U(VI) ions. It could be said that, the as prepared adsorbent had excellent adsorption capacity and good application potential for removal of uranium (VI) ions from aqueous solution.

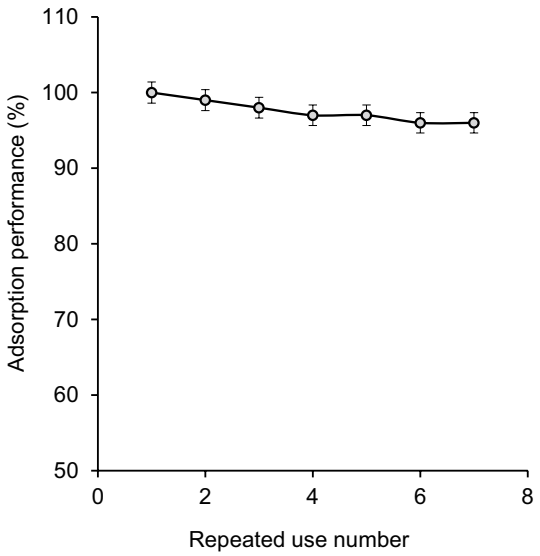


Fig. 13 Repeated use of the MA-A beads for adsorption/desorption

Conclusion

The MA-A particles were prepared and decorated with agmatine ligand and used to remove U(VI) ions. The adsorbent was characterized by FTIR, XRD, SEM and EDXS, analysis. The adsorption studies also confirmed its remarkable magnetic properties and excellent dispersion ability. The experimental data showed that MA-A beads displayed high adsorption capacities for U(VI) ions 451.4 mg/g at 25 °C. The MA-A beads illustrated good adsorption performance for uranyl ions at pH 6.5. The present study showed that the adsorption capacities of the MA-A beads for U(VI) were increased 6.4 folds after modification with agmatine. Thus, the attachment of agmatine ligand on the MA beads highly improved the adsorption capacity of U(VI) ions. The adsorption isotherms and kinetic studies showed that the Langmuir isotherm and pseudo-second-order model better described the removal of U(VI) ions on the adsorbents. In the simulated seawater, the U(VI) ions removal performance of the MA-A beads increased from 69 to 96% as the concentration of uranyl ions increased. The MA-A beads revealed good reusability during repeated adsorption/desorption cycles, and the adsorption capacity decreased about 4% for adsorption of U(VI) after seven cycles. Furthermore,

Table 5 Comparison of adsorption capacity MA-A beads with different adsorbents

Adsorbent	Medium pH	Contact time (min)	Adsorption capacity U(VI) mg/g	References
Amidoximated polyacrylonitrile -graphene oxide	5.0	90	345.1	2
Poly(tetraethylenepentamine–trimesoyl chloride	5.0	80	189.8	50
Tetraphenyldithiodiphosphonate	6.0	20	398.8	51
Poly(cyclotriphosphazene-co-polyethyleneimine) microspheres	5.0	60	274.2	52
Phospho-enriched amidoxime adsorbents	6.0	400	243.9	53
Cellulose–COOH/cellulose–NH_2 beads	6.0/5.0	60	462.9/127.4	54
Oxime-functionalized PCN-222	6.0	360	403.4	55
Polyethylenimine-functionalized carboxylated chitosan/oxidized activated charcoal composite	4.0	300	450.0	56
Chitosan grafted titanium dioxide	6.0	60	163.2	57
Agmatine ligand functionalized magnetic alginate beads	6.5	60	451.4	In this work

different functional groups could be generated on the surface of the MA beads for future applications, such as removing organic and inorganic pollutants from aqueous solutions. In conclusion, using MA beads and an amine group-rich ligand, a facile and sustainable method was used to create the environmentally friendly MA-A adsorbent to absorb different U(VI) ions effectively.

Author contributions Gulay Bayramoglu: Validation, Investigation, Formal analysis, Writing—original draft, Writing—review & editing. M. Yakup Arica: Writing—review & editing.

Funding Open access funding provided by the Scientific and Technological Research Council of Türkiye (TÜBİTAK).

Data availability All data and materials are true and valid and can use general repositories saving, and data are also provided upon request.

Declarations

Conflict of interest The authors declare that they have no known competing financial interests or personal relationships that could have appeared to influence the work reported in this paper.

Consent for publication All authors have given consent for publication.

Open Access This article is licensed under a Creative Commons Attribution 4.0 International License, which permits use, sharing, adaptation, distribution and reproduction in any medium or format, as long as you give appropriate credit to the original author(s) and the source, provide a link to the Creative Commons licence, and indicate if changes were made. The images or other third party material in this article are included in the article's Creative Commons licence, unless indicated otherwise in a credit line to the material. If material is not included in the article's Creative Commons licence and your intended use is not permitted by statutory regulation or exceeds the permitted use, you will need to obtain permission directly from the copyright holder. To view a copy of this licence, visit http://creativecommons.org/licenses/by/4.0/.

References

1. Arica MY, Bayramoglu G (2016) MCM-41 silica particles grafted with polyacrylonitrile: modification in to amidoxime and carboxyl groups for enhanced uranium removal from aqueous medium. Micropor Mesopor Mater 226:117–124. https://doi.org/10.1016/j.micromeso.2015.12.040
2. Ashrafi F, Firouzzare M (2021) Preparation of forcespun amidoximated polyacrylonitrile-graphene oxide nanofibers and evaluation of their uranium uptake from aqueous media. Fiber Polym 22:3289–3297. https://doi.org/10.1007/s12221-021-0133-8
3. Banala UK, Das NPI, Toleti SR (2021) Microbial interactions with uranium: towards an effective bioremediation approach. Environ Technol Inno 21:101254. https://doi.org/10.1016/j.eti.2020.101254
4. Koppula S, Jagasia P, Panchangam MK, Surya SBM (2022) Synthesis of bimetallic metal-organic frameworks composite for the removal of Copper(II), Chromium(VI), and Uranium(VI) from the aqueous solution using fixed-bed column adsorption. J Solid State Chem 312:123168. https://doi.org/10.1016/j.jssc.2022.123168
5. Erkaya IA, Arica MY, Akbulut A, Bayramoglu G (2014) Biosorption of uranium(VI) by free and entrapped *Chlamydomonas reinhardtii*: kinetic, equilibrium and thermodynamic studies. J Radioanal Nucl Chem 299:1993–2003. https://doi.org/10.1007/s10967-014-2964-x
6. Lilhare S, Mathew SB, Singh AK, Sankarasubramanian S (2023) A simple spectrophotometric study of adsorption of Hg(II) on glycine functionalized magnetic nanoparticle entrapped alginate beads. Int J Environ Anal Chem 103:1917–1937. https://doi.org/10.1080/03067319.2021.1884242
7. Ivanov NP, Dran'kov AN, Shichalin OO, Lembikov AO, Buravlev IY, Mayorov VY, Balanov MI, Rogachev KA, Kaspruk GD, Pisarev SM, Marmaza PA, Rastorguev VL, Balybina VA, Fedorets AN, Kaptakov VO, Papynov EK (2024) Composite magnetic sorbents based on magnetic Fe_3O_4 coated by Zn and Al layered double hydroxide for U(VI) removal from aqueous media. J Radioanal Nucl Chem. https://doi.org/10.1007/s10967-024-09362-4
8. Zhang Y, Cai T, Zhao Z, Bing H (2024) Chitosan-poly(imide dioxime) semi-interpenetrating network hydrogel for efficient uranium recovery from seawater. J Radioanal Nucl Chem 333:31–41. https://doi.org/10.1007/s10967-023-09264-x

9. Patel K, Sutar AK, Maharana T (2022) Synthesis of carboxylic graphene oxide-carboxymethyl chitosan composite and its applications toward the remediation of U^{6+}, Pb^{2+}, Cr^{6+}, and Cd^{2+} ions from aqueous solutions. J Chin Chem Soc 69:2027–2041. https://doi.org/10.1002/jccs.202200369
10. Bai J, Li S, Ma X, Yan H, Su S, Wang S, Wang J (2022) Novel preparation of amidoxime functionalized hyper-cross-linked polymeric adsorbent on the efficient adsorption of uranium in aqueous solution. Micropor Mesopor Mater 331:111647. https://doi.org/10.1016/j.micromeso.2021.111647
11. Bi C, Zhang C, Ma F, Zhang X, Yang M, Nian J, Liu L, Dong H, Zhu L, Wang Q, Guo S, Lv Q (2021) Growth of a mesoporous Zr-MOF on functionalized graphene oxide as an efficient adsorbent for recovering uranium (VI) from wastewater. Micropor Mesopor Mater 323:11223. https://doi.org/10.1016/j.micromeso.2021.111223
12. Bayramoglu G, Arica MY (2021) Grafting of regenerated cellulose films with fibrous polymer and modified into phosphate and sulfate groups: application for removal of a model azo-dye. Colloid Surf A: Physicochem Eng Asp 614:126173. https://doi.org/10.1016/j.colsurfa.2021.126173
13. Yi X, He J, Guo Y, Han Z, Yang M, Jin J, Gu J, Ou M, Xu X (2018) Encapsulating Fe_3O_4 into calcium alginate coated chitosan hydrochloride hydrogel beads for removal of Cu(II) and U(VI) from aqueous solutions. Ecotoxicol Environ Saf 147:699–707. https://doi.org/10.1016/j.ecoenv.2017.09.036
14. Bayramoglu G, Arica MY (2017) Polyethylenimine and tris(2-aminoethyl)amine modified p(GA–EGMA) microbeads for sorption of uranium ions: equilibrium, kinetic and thermodynamic studies. J Radioanal Nucl Chem 312:293–303. https://doi.org/10.1007/s10967-017-5216-z
15. Bayramoglu G, Kilic M, Arica MY (2023) *Tramates trogii* biomass in carboxymethylcellulose-lignin composite beads for adsorption and biodegradation of bisphenol A. Biodegradation 34:263–281. https://doi.org/10.1007/s10532-023-10024-7
16. Deshmukh P, Sar SK (2023) Efficient separation of uranium from aqueous solution using sustainable biomass: an insight of adsorption isotherm and kinetics. J Radioanal Nucl Chem 332:4617–4627. https://doi.org/10.1007/s10967-023-08861-0
17. Arica MY, Bayramoglu G (2016) Polyaniline coated magnetic carboxymethylcellulose beads for selective removal of uranium ions from aqueous solution. J Radioanal Nucl Chem 310:711–724. https://doi.org/10.1007/s10967-016-4828-z
18. Yadav S, Asthana A, Singh AK, Chakraborty R, Vidya SS, Susan MdABH, Carabineiro SAC (2021) Adsorption of cationic dyes, drugs and metal from aqueous solutions using a polymer composite of magnetic/β-cyclodextrin/activated charcoal/Na alginate: isotherm, kinetics and regeneration studies. J Hazard Mater 409:124840. https://doi.org/10.1016/j.jhazmat.2020.124840
19. Facchia DP, Cazettac AL, Canesina EA, Almeidac VC, Bonaféa EG, Kipperd MJ, Martinsa AF (2018) New magnetic chitosan/alginate/ Fe_3O_4@SiO_2 hydrogel composites applied for removal of Pb(II) ions from aqueous systems. Chem Eng J 337:595–608. https://doi.org/10.1016/j.cej.2017.12.142
20. Lilhare S, Mathew SB, Singh AK, Carabineiro SAC (2021) Calcium alginate beads with entrapped iron oxide magnetic nanoparticles functionalized with methionine—A versatile adsorbent for arsenic removal. Nanomaterials 11:1345. https://doi.org/10.3390/nano11051345
21. Hattali A, Bouras O, Hanini S (2023) Sorption efficiency of Pb^{2+} ions using (bio) nano-composite magnetic gelled beads. Mater Today Proc 78:760–766. https://doi.org/10.1016/j.matpr.2022.10.233
22. Alves LC, Yanez-Vilar S, Pineiro-Redondo Y, Rivas J (2020) Efficient separation of heavy metals by magnetic nanostructured beads. Inorganics 8:40. https://doi.org/10.3390/inorganics8060040
23. Arica TA, Balci FM, Balci S, Arica MY (2022) Highly porous poly (o-phenylenediamine) loaded magnetic carboxymethyl cellulose hybrid beads for removal of two model textile dyes. Fiber Polym 23:2838–2854. https://doi.org/10.1007/s12221-022-0221-4
24. Talbot D, Abramson S, Griffete N, Bée A (2018) pH-sensitive magnetic alginate/γ-Fe_2O_3 nanoparticles for adsorption/desorption of a cationic dye from water. J Water Process Eng 25:301–308. https://doi.org/10.1016/j.jwpe.2018.08.013
25. Arica TA, Ayas E, Arica MY (2017) Magnetic MCM-41 silica particles grafted with poly(glycidylmethacrylate) brush: modification and application for removal of direct dyes. Micropor Mesopor Mater 243:164–175. https://doi.org/10.1016/j.micromeso.2017.02.011
26. Ahmadpoor F, Shojaosadati SA, Mousavi Z (2019) Magnetic silica coated iron carbide/alginate beads: synthesis and application for adsorption of Cu(II) from aqueous solutions. Int J Biol Macromol 128:941–947. https://doi.org/10.1016/j.ijbiomac.2019.01.173
27. Wang B, Wan Y, Zheng Y, Lee X, Liu T, Yu Z, Huang J, Ok YS, Chen J, Gao B (2019) Alginate-based composites for environmental applications: a critical review. Crit Rev Environ Sci Technol 49:318–356. https://doi.org/10.1080/10643389.2018.1547621
28. Cojocaru C, Humelnicu AC, Samoila P, Petronela P, Harabagiu V (2018) Optimized formulation of $NiFe_2O_4$@Ca-alginate composite as a selective and magnetic adsorbent for cationic dyes: experimental and modeling study. React Funct Polym 125:57–69. https://doi.org/10.1016/j.reactfunctpolym.2018.02.008
29. Elwakeel KZ, Hamza MF, Guibal E (2021) Effect of agitation mode (mechanical, ultrasound and microwave) on uranium sorption using amine- and dithizone-functionalized magnetic chitosan hybrid materials. Chem Eng J 411:128553. https://doi.org/10.1016/j.cej.2021.128553
30. Celikbıcak O, Bayramoglu G, Acıkgoz-Erkaya I, Arica MY (2021) Aggrandizement of uranium (VI) removal performance of *Lentinus concinnus* biomass by attachment of 2,5-diaminobenzenesulfonic acid ligand. J Radioanal Nucl Chem 328:1085–1098. https://doi.org/10.1007/s10967-021-07708-w
31. Bayramoglu G, Cimen AG, Arica MY (2024) Amidoxime-functionalized magnetic graphene oxide-silica particles for adsorption of U(VI) ions from an aqueous medium. J Radioanal Nucl Chem 333:585–597. https://doi.org/10.1007/s10967-023-09254-z
32. Deng M, Ai Y, Zhao L, Xu Y, Ouyang Y, Yang P, Peng G (2021) Preparation of NH_2-CTS/MZ composites and their adsorption behavior and mechanism on uranium ions. J Radioanal Nucl Chem 330:963–978. https://doi.org/10.1007/s10967-021-07991-7
33. Zheng XY, Shen YH, Wang XY, Wang TS (2018) Effect of pH on uranium(VI) biosorption and biomineralization by Saccharomyces cerevisiae. Chemosphere 203:109–116. https://doi.org/10.1016/j.chemosphere.2018.03.165
34. Xiao F, Cheng Y, Zhou P, Chen S, Wang X, He P, Nie X, Dong F (2021) Fabrication of novel carboxyl and amidoxime groups modified luffa fiber for highly efficient removal of uranium (VI) from uranium mine water. J Environ Chem Eng 9:105681. https://doi.org/10.1016/j.jece.2021.105681
35. Beni AA (2021) Design of a solar reactor for the removal of uranium from simulated nuclear wastewater with oil-apatite ELM system. Arabian J Chem 14:102959. https://doi.org/10.1016/j.arabjc.2020.102959
36. Zhang G, Wang Y, Zhang X, Liu L, Ma F, Zhang C, Dong H (2022) Synthesis of a porous amidoxime modified hypercrosslinked benzil polymer and efficient uranium extraction from water. Colloid Surf A 641:128508. https://doi.org/10.1016/j.colsurfa.2022.128508

37. Chen J, Gao J, Lv H, Wen Q, Han J, Liu P, Yan Y, Xue Y, Ma F (2023) Preparation of polydopamine-functionalized polyamidoxime membrane for uranium recovery from seawater. Appl Surf Sci 634:157604. https://doi.org/10.1016/j.apsusc.2023.157604
38. Kanjilal A, Singh KK, Tyagi AK, Dey GR (2021) Synthesis of bifunctional chelating sorbent for recovery of uranium from aqueous solution: sorption, kinetics and reusability studies. J Polym Res 28:460. https://doi.org/10.1007/s10965-021-02819-0
39. Bayramoglu G, Angi SB, Acikgoz-Erkaya I, Arica MY (2022) Preparation of effective green sorbents using O. Princeps alga biomass with different composition of amine groups: comparison to adsorption performances for removal of a model acid dye. J Mol Liq 347:118375. https://doi.org/10.1016/j.molliq.2021.118375
40. Song Y, Wei G, Kopec M, Rao L, Zhang Z, Gottlieb E, Wang Z, Yuan R, Ye G, Wang J, Kowalewski T, Matyjaszewski K (2018) Copolymer-templated synthesis of nitrogen-doped mesoporous carbons for enhanced adsorption of hexavalent chromium and uranium. ACS Appl Nano Mater 1:2536–2543. https://doi.org/10.1021/acsanm.8b00103
41. Bayramoglu G, Erkaya-Acikgoz I, Akbulut A, Arica MY (2023) Removal of various phenolic compounds from solution using free and entrapped *Lentinus sajor-caju*. Int J Environ Sci Technol 20:9001–9012. https://doi.org/10.1007/s13762-023-05042-0
42. Freundlich H (1907) Über die Adsorption in Lösungen". Zeitschrift für Physikalische Chemie-Stöchiometrie und Verwandschaftslehre 57:385–470. https://doi.org/10.1515/zpch-1907-5723
43. Bayramoglu G, Arica MY (2019) Star type polymer grafted and polyamidoxime modifed silica coated-magnetic particles for adsorption of U(VI) ions from solution. Chem Eng Res Des 147:146–159. https://doi.org/10.1016/j.cherd.2019.04.039
44. Zhang X, Zhang J, Peng Y, Wu X, Li M, Wen H, Sun Z, Ye J, Hua Y (2022) Synergistic removal of glyphosate and U(VI) from aqueous solution by goethite: adsorption behavior and mechanism. J Radioanal Nucl Chem 331:1807–1819. https://doi.org/10.1007/s10967-022-08223-2
45. Lagergren S (1898) Zur theorie der sogenannten. Adsorption gel oster stoffe, Kungliga Svenska Vetenskapsakademiens, Handlingar 25:1–39
46. Ho YS, McKay G (1999) Pseudo-second-order model for sorption processes. Process Biochem 34:451–465. https://doi.org/10.1016/S0032-9592(98)00112-5
47. Bayramoglu G, Arica MY (2005) Ethylenediamine grafted poly (glycidylmethacrylate-co-methylmethacrylate) adsorbent for removal of chromate anions. Sep Pur Technol 45:192–199. https://doi.org/10.1016/j.seppur.2005.03.009
48. Liu F, Hu J, Hu B (2022) Magnetic MXene-NH_2 decorated with persimmon tannin for highly efficient elimination of U(VI) and Cr(VI) from aquatic environment. Int J Biol Macromol 219:886–896. https://doi.org/10.1016/j.ijbiomac.2022.08.034
49. Chen W, Feng J, Liu S, Zhang J, Cai Y, Lv Z, Fang M, Tan X (2022) A green and economical MgO/biochar composite for the removal of U(VI) from aqueous solutions. Chem Eng Res Des 180:391–401. https://doi.org/10.1016/j.cherd.2022.02.031
50. Peng T-Q, Wang Y-F, Xu Y-F, Liu Z-C (2023) Synthesis, characterization and uranium (VI) adsorption mechanism of novel adsorption material poly(tetraethylenepentamine–trimesoyl chloride). J Radioanal Nucl Chem 332:409–422. https://doi.org/10.1007/s10967-022-08739-7
51. Liu Z, Wang Y, Xu Y, Peng T (2024) Adsorption of uranium(VI) in aqueous solution by tetraphenyldithiodiphosphonate. J Radioanal Nucl Chem 333:357–373. https://doi.org/10.1007/s10967-023-09266-9
52. Xie X, Wang Y, Xiong Z, Li H, Yao C (2020) Highly efficient removal of uranium(VI) from aqueous solution using poly(cyclotriphosphazene-co-polyethyleneimine) microspheres. J Radioanal Nucl Chem 326:1867–1877. https://doi.org/10.1007/s10967-020-07455-4
53. Lei F, Zhou Y, Geng L, Li B, Chen J, Liu Y, Hu Y, Liu T, Shi K, Wu W, Yang J (2024) Phospho-Enriched amidoxime adsorbents utilizing synergistic multifunctional groups for enhanced uranium removal from wastewater. Chem Eng J 488:151045. https://doi.org/10.1016/j.cej.2024.151045
54. Bayramoglu G, Tilki S, Arica MY (2024) Preparation of amine or carboxyl groups modified cellulose beads for removal of uranium (VI) ions from aqueous solutions. Cellulose. https://doi.org/10.1007/s10570-024-05909-6
55. Bi C, Zhang C, Wang C, Zhu L, Zhu R, Liu L, Wang Y, Ma F, Dong H (2024) Construction of oxime-functionalized PCN-222 based on the directed molecular structure design for recovering uranium from wastewater. Environ Sci Pollut Res 31:16554–16570. https://doi.org/10.1007/s11356-024-32208-1
56. Shen J, Cao F, Liu S, Wang C, Chen R, Ke C (2022) Effective and selective adsorption of uranyl ions by porous polyethylenimine-functionalized carboxylated chitosan/oxidized activated charcoal composite. Front Chem Sci Eng 16:408–419. https://doi.org/10.1007/s11705-021-2054-x
57. Wang J, Huo Y, Ai Y (2020) Experimental and theoretical studies of chitosan modified titanium dioxide composites for uranium and europium removal. Cellulose 27:7765–7777. https://doi.org/10.1007/s10570-020-03337-w

Publisher's Note Springer Nature remains neutral with regard to jurisdictional claims in published maps and institutional affiliations.